Graphical Models 116 (2021) 101113

Contents lists available at ScienceDirect

Graphical Models

journal homepage: www.elsevier.com/locate/gmod

Scale-Adaptive ICP☆

Yusuf Sahillioğlu [*,a], Ladislav Kavan [b]

[a] Middle East Technical University, Computer Engineering Department, Ankara, Turkey
[b] University of Utah, School of Computing, Salt Lake City, Utah, USA

ARTICLE INFO

Keywords:
Pairwise registration
Shape registration
Shape alignment
Scale-adaptive

ABSTRACT

We present a new scale-adaptive ICP (Iterative Closest Point) method which aligns two objects that differ by rigid transformations (translations and rotations) and uniform scaling. The motivation is that input data may come in different scales (measurement units) which may not be known a priori, or when two range scans of the same object are obtained by different scanners. Classical ICP and its many variants do not handle this scale difference problem adequately. Our novel solution outperforms three different methods that estimate scale prior to alignment and a fourth method that, similar to ours, jointly optimizes for scale during the alignment.

1. Introduction

Scale-adaptive ICP (Iterative Closest Point) presented in this paper aligns a pair of objects that differ by rigid transformations (translations and rotations) and uniform scaling. Classical ICP [4] and its numerous variants [35] as well as the more recent noise-insensitive versions [26] do not properly handle scale differences. The naïve solution of pre-scaling the input pair prior to registration is generally not sufficient (Fig. 1). Our main contribution is to provide a principled solution to this problem by integrating the scale factor directly into the least-squares problem. This novel approach is different from the common way of decoupling the scaling optimization from the process via a prior scale estimation. Being well studied for a pair of shapes under the same scaling, this registration problem is yet at its infancy when arbitrary scaling is present. We believe that our solution can be useful for many computer graphics applications including the following ones:

- Objects to be rigidly aligned, or registered, may naturally come in different scales, e.g., when rigid registration is used to generate the initialization of a non-rigid alignment [38], or when two range scans of the same object are obtained by different scanners.
- Given a target unrigged mesh and multiple source rigs from different characters, one can register the source rigged parts to the target mesh and transfer their skinning information, creating a fully rigged and skinned character [29].
- 3D reconstructions based on structure-from-motion algorithms [6] and hyperscpectral images [51] lead to inconsistent scales at different views and spectral bands. One consequently requires a scale adaptation before merging them to a complete 3D model.
- Real-time 3D scans during a surgical operation might be required to be registered to a preoperative CT scan that is not necessarily at the same scale.
- In order to replace a small broken part of a large 3D print, one acquires the digital model of the physical object and aligns it to the original arbitrarily-scaled 3D model to identify the broken part for a re-print.

Our goal is to transform a (moving) point set S_1 towards a fixed (target) point set S_2. We follow the original ICP framework which alternates between correspondence and transformation optimizations. Specifically, given the correspondence according to the closest point matches between S_1 and S_2, ICP computes the optimal rotation and translation jointly. The transformed points imply new, and hopefully better, closest point correspondences that lead to an even better transformation in the next iteration. We take the rotation from this framework and jointly optimize for translation and uniform scaling, which adapts the scale of S_1 to that of S_2 within the process.

In all the subsequent figures, we paint transforming S_1 in green and fixed S_2 in red. We note that the source code and the executables for the method that we present in this paper are publicly available at http://www.ceng.metu.edu.tr/~ys/pubs/ScaleAdaptiveICP.zip. Our supplementary video also reveals animated results that show our execution from start to convergence: http://www.ceng.metu.edu.tr/~ys/pubs/sicp.mp4.

☆ This work was supported by TUBITAK under the project EEEAG-115E471 and by NSF under IIS-1617172, IIS-1622360 and IIS-1764071
* Corresponding author.
E-mail addresses: ys@ceng.metu.edu.tr (Y. Sahillioğlu), ladislav.kavan@gmail.com (L. Kavan).

https://doi.org/10.1016/j.gmod.2021.101113
Received 11 December 2020; Received in revised form 5 April 2021; Accepted 21 May 2021
Available online 28 May 2021

2. Related work

Since the introduction of the pioneering Iterative Closest Point (ICP) paper for rigid shape registration [4], a vast study has been carried out in the literature to extend it in many aspects [10,35,41]. Despite their different work flows, all these studies aim to find the optimal rigid transformation in terms of a rotation and a translation. We compute the additional uniform scaling factor within this well-established framework. Note that when shapes to be aligned are fully similar, as opposed to the more common partial similarity scenario in ICP, one can handle scaling issue trivially by normalizing global properties such as the diagonal of the bounding boxes, maximum distances (used in our paper for comparisons), and ratio of the root-mean-square deviations of the coordinates from their centroids [19] (also used in our comparison suite).

ICP algorithm first matches the closest points between two input point sets. Based on the matching it computes and applies the optimal rigid transformation, and repeats the process iteratively. A common modification to ICP suggests changing the original point matching criterion from point-to-point distances to point-to-plane distances [7,8,23,31] and symmetrized point-to-plane distances [34], which allow faster tangential movement of the surfaces. Features such as integral descriptors [32] and geometric descriptors [2] accelerate ICP by reducing the transformation search space. For the same purpose, random sample consensus (RANSAC) mechanism that considers three-point or four-point [1,27,30] tuples is also adapted to the ICP framework. Additional visual appearance information is also used in the registration of RGB-D data [14]. In this scenario, the keypoint descriptors [3,33] are expected to be invariant to illumination.

A notorious problem with the ICP-based techniques is getting stuck in local minima of the alignment error function. Several methods that alleviate this problem employ multi-resolution strategies [20], genetic algorithms [39], branch-and-bound techniques [46], and robust dense objective functions [50] in order to search the entire 3D motion space in an efficient manner.

ICP modifications are also affected by the recent popularization of deep learning techniques. Local 3D geometric structures are encoded using a deep neural network auto-encoder [15], a 3D fully-convolutional network [9], or a siamese deep learning architecture [17] instead of employing traditional descriptors, which in turn leads to superior results on challenging noisy point cloud registration datasets[21]., on the other hand, uses their learned compact descriptor in the framework of [50] for better precision. Other descriptor learning methods [47,49] cooperate with the RANSAC search algorithm to produce point cloud registrations.

There exist only a few methods that aim to address the scaling issue. The first one [52] solves for rotation, scaling, and translation independently in this order[13]., and its extensions by the same research group Du et al. [11,12,22,48], inject the scale matrix directly into the ICP least-squares problem with a constraint condition that the matrix is bounded. Although it is not demonstrated in their result sets, the reason of finding a scaling matrix instead of a scaling factor is to handle non-uniform scaling. Since matrix search complicates the process, we stick with the search of the uniform scale factor scalar, which already has many use cases as listed in Section 1. They also had to optimize the rotation and scaling matrices jointly, which is different and more complicated than our joint optimization on scaling and translation. Although both these methods, like our method, report execution times as fast as the standard ICP, they do not clearly provide the final linear system they solve, which makes their reproduction difficult. We, on the other hand, derive our linear system step by step and present it clearly in one equation (Eq. 6) and also share our code and executables publicly. Our evaluation is also more comprehensive than that of the existing works, e.g., we in fact fail to see *partially* similar cases in their entire result sets. As we stated previously, when shapes are fully, not partially, similar, much more trivial solutions arise to normalize shape scales [19]. More recently, combination of local descriptors at different scales [24,25], PCA of spin images over different scales [42], and the growing least-squares descriptor [28] help estimating the relative scale between two *fully* similar shapes prior to their alignment. The most recent technique in this line of work [45] decouples scale, rotation and translation estimation. Their initial uniform scale factor estimation based on FPFH correspondences [36] is made robust to outliers by an adaptive voting scheme. This robustness in turn renders the work as well as its

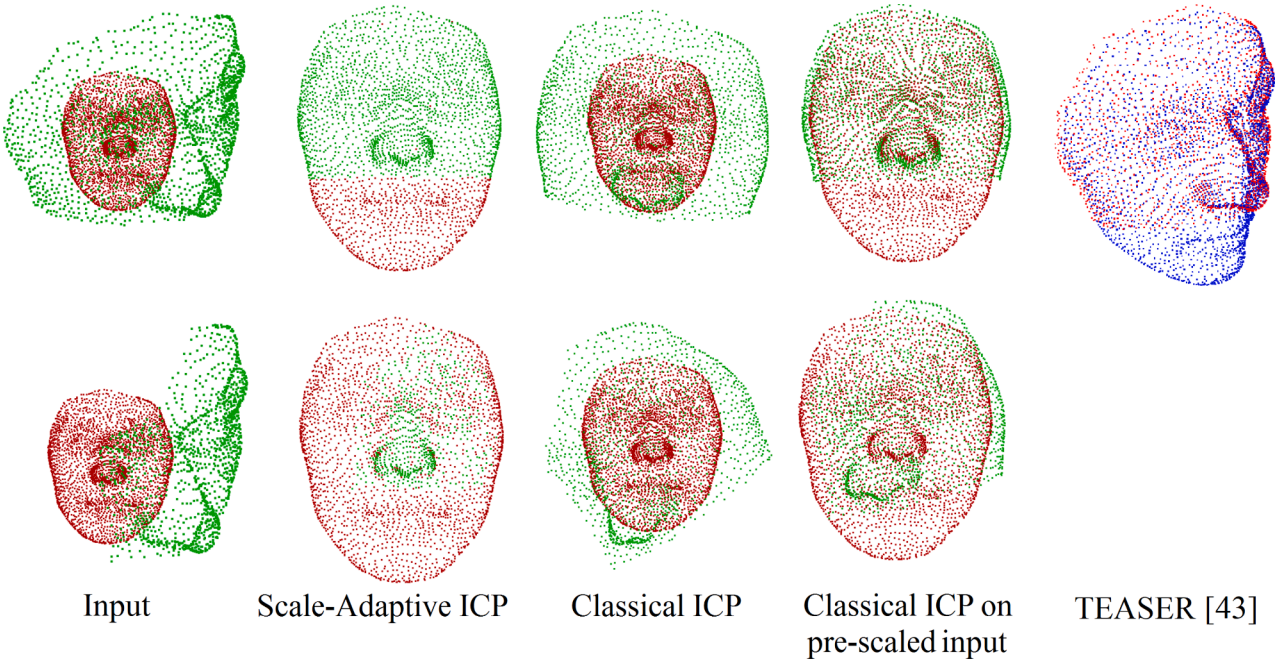

Fig. 1. Rigid registration based on our Scale-Adaptive ICP, Classical ICP, and Classical ICP with a naïve prior scaling, which is carried out by multiplying the points of the first set S_1 by a/b where a and b are the distances between two farthest points of S_2 and S_1, respectively. When shapes are only partially similar, farthest points are likely to be incompatible which in turn leads to normalization errors (see also Fig. 11 and the supplementary video). Coinciding red and green points are painted arbitrarily (z-fighting issue) in this figure and the subsequent ones. A more sophisticated pre-scaling by the current state-of-the-art [45] is shown at right.

preliminary study [44] suitable for the more challenging partial similarity case.

The most recent work of Du et al. [43] replaces the mean square error with a correntropy criterion as a new similarity measure with the main purpose of eliminating the interference of outliers and noises. While being able to estimate a scale factor after a relatively slow process that requires computation of the real exponential function, their method, like their prior work, fail to provide clear demonstrations and evaluations, e.g., intermediate results during iterations are missing. The method is also reported to be sensitive to the kernel bandwidth that defines the correntropy.

3. The algorithm

Let $\mathbf{p}_i \in S_1$ be the source point to be aligned with the fixed corresponding target point $\mathbf{q}_i \in S_2$ for $i \in [1,n]$ where n is the number of points on the source object. Having computed the optimal rotation $\mathbf{R}$ via the closed-form expression in [4], we have $\mathbf{p}_i' = \mathbf{R}\mathbf{p}_i$ as the ICP-rotated point. While the classical ICP and its variants simply apply the next transformation as the optimal translation $\mathbf{u}$ that moves the centroid of the rotated source points to the centroid of the fixed target points, we instead jointly optimize for the translation $\mathbf{t}$ and the uniform scale factor s. The optimal s and the optimal $\mathbf{t}$, that is not necessarily the same as $\mathbf{u}$, are then applied to $\mathbf{p}_i'$ at each iteration of the classical ICP framework, yielding the results in Fig. 1-second column and in Section 4. We derive s and $\mathbf{t}$ in the sequel.

We are seeking $s \in \mathbb{R}$ and $\mathbf{t} \in \mathbb{R}^{3\times 1}$ that minimize $E(s,\mathbf{t}) = \sum_{i=1}^{n} \| (s\mathbf{p}_i' + \mathbf{t}) - \mathbf{q}_i \|^2$. Notice that if we take $s = 1$ as in all other ICP methods, we find the optimal translation as $\mathbf{t} = \overline{\mathbf{q}} - \overline{\mathbf{p}'}$, where $\overline{\mathbf{p}'}$ and $\overline{\mathbf{q}}$ are the centroids of the rotated source points and fixed target points, respectively.

We begin by converting $E(s,\mathbf{t})$ to the following form that is suitable for differentiation.

$$\begin{aligned} E(s,\mathbf{t}) &= \sum_{i=1}^{n} \left((s\mathbf{p}_i' + t) - \mathbf{q}_i\right)^{\mathsf{T}} \left((s\mathbf{p}_i' + t) - \mathbf{q}_i\right) \\ &= \sum_{i=1}^{n} \left(s\mathbf{p}_i' + t\right)^{\mathsf{T}} \left(s\mathbf{p}_i' + t\right) - 2\left(s\mathbf{p}_i' + t\right)^{\mathsf{T}} \mathbf{q}_i + \mathbf{q}_i^{\mathsf{T}}\mathbf{q}_i \\ &= \sum_{i=1}^{n} \left(s\mathbf{p}_i'\right)^{\mathsf{T}} \left(s\mathbf{p}_i'\right) + 2\left(s\mathbf{p}_i'\right)^{\mathsf{T}}\mathbf{t} + \mathbf{t}^{\mathsf{T}}\mathbf{t} - 2\left(s\mathbf{p}_i'\right)^{\mathsf{T}}\mathbf{q}_i \\ &\qquad -2\mathbf{t}^{\mathsf{T}}\mathbf{q}_i + \mathbf{q}_i^{\mathsf{T}}\mathbf{q}_i \\ &= \sum_{i=1}^{n} \left(\mathbf{p}_i'\right)^{\mathsf{T}} s^{\mathsf{T}} s\mathbf{p}_i' + 2\left(\mathbf{p}_i'\right)^{\mathsf{T}} s^{\mathsf{T}}\mathbf{t} + \mathbf{t}^{\mathsf{T}}\mathbf{t} - 2\left(\mathbf{p}_i'\right)^{\mathsf{T}} s^{\mathsf{T}}\mathbf{q}_i \\ &\qquad -2\mathbf{t}^{\mathsf{T}}\mathbf{q}_i + \mathbf{q}_i^{\mathsf{T}}\mathbf{q}_i \end{aligned} \tag{1}$$

We then set the partial derivatives to zero for minimization:

$$\partial E/\partial s = 2s\sum_{i=1}^{n} \left(\mathbf{p}_i'\right)^{\mathsf{T}}\mathbf{p}_i' + 2\sum_{i=1}^{n} \left(\mathbf{p}_i'\right)^{\mathsf{T}}\mathbf{t} - 2\sum_{i=1}^{n} \left(\mathbf{p}_i'\right)^{\mathsf{T}}\mathbf{q}_i = 0 \tag{2}$$

$$\begin{aligned} \partial E/\partial \mathbf{t} &= 2\sum_{i=1}^{n} \left(\mathbf{p}_i'\right)^{\mathsf{T}} s^{\mathsf{T}} + 2\sum_{i=1}^{n} \mathbf{t} - 2\sum_{i=1}^{n} \mathbf{q}_i \\ &= 2s\sum_{i=1}^{n} \mathbf{p}_i' + 2n\mathbf{t} - 2\sum_{i=1}^{n} \mathbf{q}_i = 0 \end{aligned} \tag{3}$$

Rewriting Eq. 2 yields

$$\begin{aligned} \sum_{i=1}^{n} \left(\mathbf{p}_i'\right)^{\mathsf{T}}\mathbf{q}_i &= s\sum_{i=1}^{n} \left(\mathbf{p}_i'\right)^{\mathsf{T}}\mathbf{p}_i' + \sum_{i=1}^{n} \left(\mathbf{p}_i'\right)^{\mathsf{T}}\mathbf{t} \\ &= s\sum_{i=1}^{n} \left(\mathbf{p}_i'\right)^{\mathsf{T}}\mathbf{p}_i' + \mathbf{c}\mathbf{t} \\ &= s\sum_{i=1}^{n} \left(\mathbf{p}_i'\right)^{\mathsf{T}}\mathbf{p}_i' + c_0t_0 + c_1t_1 + c_2t_2 \end{aligned} \tag{4}$$

where $\mathbf{c} \in \mathbb{R}^{1\times 3} = \sum_{i=1}^{n} (\mathbf{p}_i')^{\mathsf{T}}$.

Rewriting Eq. 3 yields

$$\sum_{i=1}^{n} \mathbf{q}_i = s\sum_{i=1}^{n} \mathbf{p}_i' + n\mathbf{t} \tag{5}$$

The linear system of Eqs. 4 and 5 is put in the following $\mathbf{A}\mathbf{x} = \mathbf{b}$ form for a fast solve.

$$\begin{bmatrix} \sum_{i=1}^{n} \left(\mathbf{p}_i'\right)^{\mathsf{T}}\mathbf{p}_i' & c_0 & c_1 & c_2 \\ c_0 & n & 0 & 0 \\ c_1 & 0 & n & 0 \\ c_2 & 0 & 0 & n \end{bmatrix} \begin{bmatrix} s \\ t_0 \\ t_1 \\ t_2 \end{bmatrix} = \begin{bmatrix} \sum_{i=1}^{n} \left(\mathbf{p}_i'\right)^{\mathsf{T}}\mathbf{q}_i \\ d_0 \\ d_1 \\ d_2 \end{bmatrix} \tag{6}$$

where $\mathbf{d} \in \mathbb{R}^{3\times 1} = \sum_{i=1}^{n} \mathbf{q}_i$.

There is a key insight to make this process work well even under significant scale differences. When S_1 is significantly underscaled relative to S_2, e.g., as in the input configurations in Fig. 2-left, closest point matches cluster around a specific region that is relatively small. The uniform scaling factor computed by our method would then shrink S_1 even more in order to respect these erroneous correspondences packed in a small region. To alleviate the problem, we enforce the closest point mapping to be one-to-one initially, which naturally spreads the target points to a larger region, hence preventing the scale factor from being unnecessarily small in the beginning. Once the displacement between two consecutive iterations becomes sufficiently small, we relax the one-to-one mapping constraint to the usual many-to-one mapping, leading to the improved results in Fig. 2.

4. Experimental results

We tested the performance of our scale-adaptive ICP algorithm for the pairwise alignment of four main object categories: Face, Stanford Bunny, Homer, and Quadruped, where the first and last ones are taken from [40], and the others have been released into the public domain. We randomly crop, rotate, and/or re-scale a point set to transform it towards

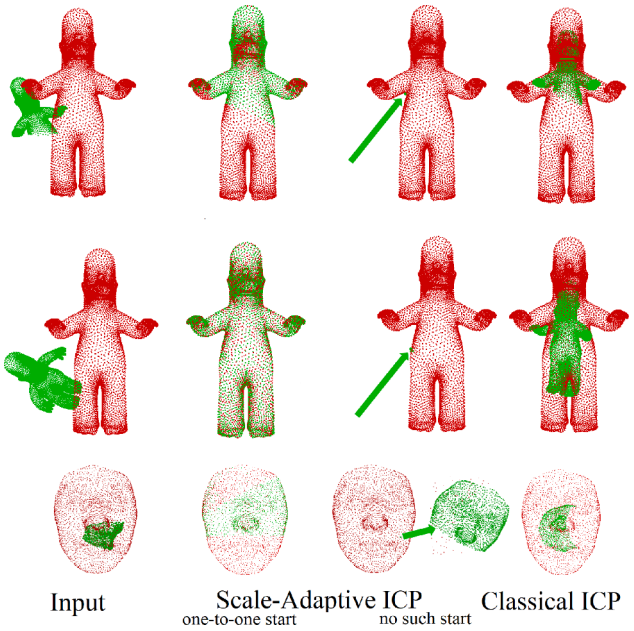

Fig. 2. Comparison of our scale-adaptive ICP results to the classical ICP results at the right. Note that, scale-adaptive ICP works better if it starts with one-to-one closest point mapping. Green arrows point to the undesired results that are shrunk.

the original reference point set.

One of the main motivations of performing scale-adaptive ICP is to register the scans of the same object captured via different scanners at possibly different times. In such a scenario, and many others including the ones listed in Section 1, scale differences are likely to arise. In the sequel, we provide our qualitative and quantitative results on this scale-difference scenario in comparison with the related work that includes the current state-of-the-art that considers scaling [45].

4.1. Comparison to correspondence-Free pre-Scaling

It is not trivial to robustly pre-scale such partially similar objects before the alignment because of the lack of corresponding points that are supposed to guide the normalization [37]. Naïve pre-scaling approaches based on maximum distances (Fig. 1-fourth column, Fig. 11-bottom, and video) and deviation ratios [19] (Fig. 3) are also shown to be unstable. The latter proposes to use the root-mean-square deviations of the coordinates from their centroids, i.e.,

$$S_1^{\text{RMS}} = \sqrt{\frac{1}{n}\sum_{i=1}^{n} \| \mathbf{p}_i - \overline{\mathbf{p}} \|^2} \qquad S_2^{\text{RMS}} = \sqrt{\frac{1}{m}\sum_{i=1}^{m} \| \mathbf{q}_i - \overline{\mathbf{q}} \|^2} \tag{7}$$

and pre-scale the point set S_1 of size n via the ratio $S_2^{\text{RMS}} / S_1^{\text{RMS}}$. Note that both the distance-based (explained in the caption of Fig. 1) and the deviation-based factors essentially measure the variance of the point distributions without requiring any correspondence information which is hard to obtain, especially in our arbitrary scaling scenario.

Once pre-scaled, classical ICP [4] handles the alignment by finding rotations and translations iteratively.

4.2. Comparison to correspondence-Based pre-Scaling

The most recent pre-scaling technique called TEASER [45] produces satisfactory results (Fig. 1-right and Fig. 4-right) when equipped with sufficiently accurate keypoint detection and matching procedures [36]. It also requires parameter-dependent downsampling to be able to complete in reasonable times (Fig. 5). The downsampling operation also slightly changes the coordinates of the points (in a sense that is equivalent to adding noise) so that it is naturally impossible to obtain zero deviation. Our qualitative (Fig. 1 and Fig. 4) and quantitative (Table 1) results are slightly better than that of this state-of-the-art method.

TEASER provides the state-of-the-art results for pre-scaling based registration because it does not simply rely on the keypoint matches which are likely to be erroneous in a challenging setting like this one.

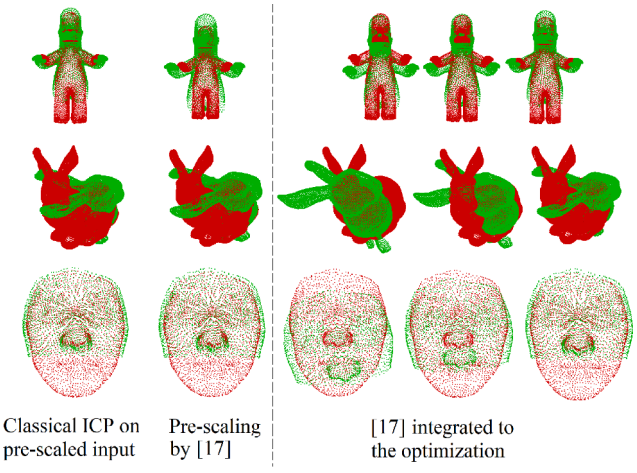

Fig. 3. (Left side of the dashed line) Classical ICP runs after the distance-based and deviation-based pre-scaling. (Right) Deviation-based pre-scaling is performed jointly during ICP iterations; 3 iterations are shown where the last one is the result.

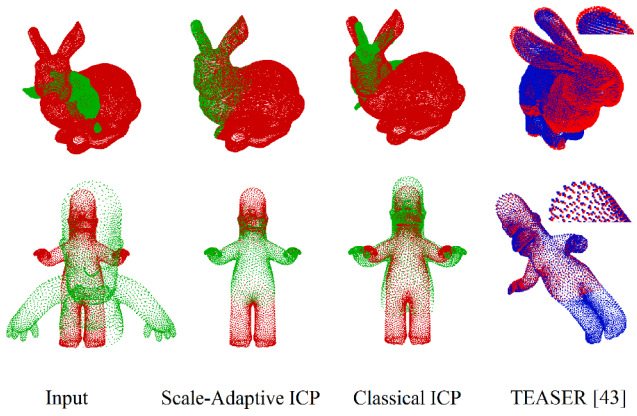

Fig. 4. Our results in comparison with the Classical ICP [4] and the state-of-the art [45]. For the latter, we show zoomed portions to depict the slight deviations from the exact overlap that we can provide.

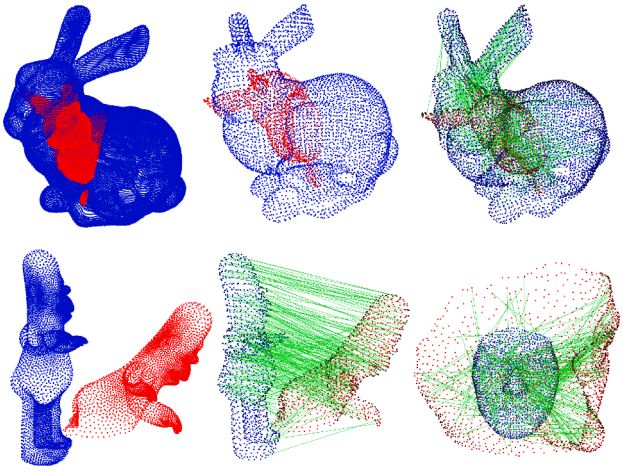

Fig. 5. (Top) Original input pair (left) needs to be downsampled (middle) and matched (right) for TEASER to work properly. (Bottom) Downsampling and matching on different pairs.

Table 1
Columns from left to right correspond to TEASER [45], classical ICP after pre-scaling by maximum distances, classical ICP after pre-scaling by [19], joint optimization by [19], and joint optimization by our method. Average spacing between points is 0.0002 (in order to interpret the results easily).

	M1	M2	M3	M4	M5
Eq. 1	0.00012	0.03139	0.02647	0.00193	1e-7

Assuming that FPFH descriptor [36], or any other descriptor, provides a sufficient number of good matches, TEASER adaptively votes for the best scale factor. The key observation in the voting process is the fact that $\| \mathbf{q}_a - \mathbf{q}_b \| \; / \; \| \mathbf{p}_c - \mathbf{p}_d \|$ is close to the true scale s if $(\mathbf{p}_c, \mathbf{q}_a)$ and $(\mathbf{p}_d, \mathbf{q}_b)$ are good matches. Consequently, good matches are clustered together since they are all close to s and hence they are all mutually close. Adaptive voting aims to detect the densest cluster in this context.

Once pre-scaled, TEASER estimates rotation and translation via their semidefinite programming relaxation and componentwise adaptive voting, respectively.

4.3. Comparison to joint scaling

Our method, free of any error-prone pre-scaling action, performs the scaling within the robust ICP framework iteratively, leading to the

improved results in Figs. 1–7 and in the supplementary video: http://www.ceng.metu.edu.tr/~ys/pubs/sicp.mp4. The only similar literature that integrates the scale factor directly into the least-squares problem is due to the group of Du et al. We, however, fail to obtain their results due to the lack of reproduction clarity, lack of public repositories, and lack of their responses to our communications. We, therefore, opt to modify the transformation optimization step in ICP with the basic deviation ratio solution proposed in [19] (Eq. 7). We outperform this baseline method (Fig. 3-right and Table 1) which is free of pre-scaling and uses joint-optimization, i.e., similar to our method, computes a new scale factor at each iteration based on the current configuration. Finally note that, we also compare with the classical ICP [4] which, in this context, gives the worst results as it is not designed to handle scaling, either via pre-scaling or joint optimization.

Note that, our algorithm naturally supports the case where there is no scale difference in the beginning (Fig. 8). It also allows the fixed reference shape (red) to be bigger or smaller that the moving shape (green). The uniform scale factor computed at each iteration is mostly larger than 1 for the former case, and less than 1 for the latter. Significant scaling occurs in the first few iterations and then the rate of change decreases as the factor converges to 1 (see Fig. 9 and the supplementary video).

Another motivation for performing scale-adaptive ICP is to provide a good initialization for the non-rigid registration task. To this end, we register different quadrupeds and facial expressions (Figs. 10 and 11).

We qualitatively evaluated our algorithm under various settings discussed thus far. Consistent with the visuals that show clear overlaps after successful alignments, the quantitative evaluation reveals an error (Eq. 1) of 1e-10 or less. Note that, Eq. 1 measures the dissimilarity between the transformed and fixed point sets in L_2 norm. When all 20 test pairs are considered in each category this error averages to about 1e-7 (see Section 5). We wrap up all the resulting errors in Table 1. We also show that our good performance is maintained under geometric noise and extended partiality where the target point set is also cropped (Fig. 12 and Table 2). Eq. 1 naturally increases in the latter case as the correspondences of some of the moving points are now cropped.

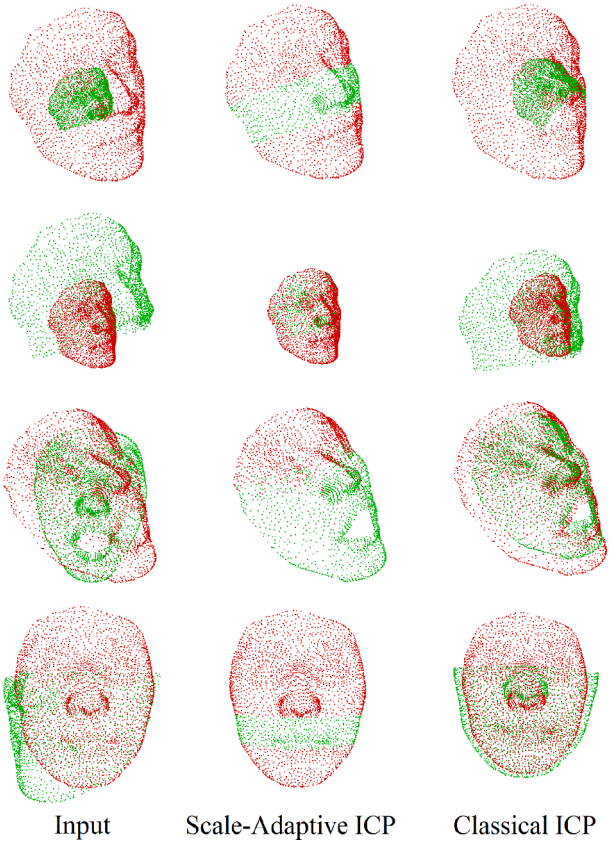

Fig. 6. Cropped, rotated, and/or scaled version (green) of the reference shape (red) is registered via our method (middle) and the classical method (right). (For interpretation of the references to colour in this figure legend, the reader is referred to the web version of this article.)

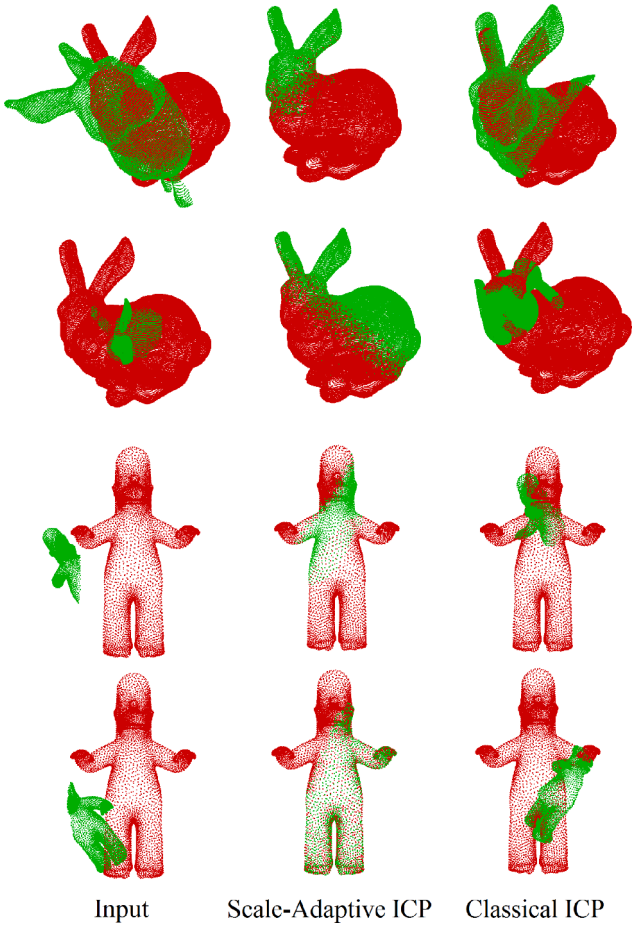

Fig. 7. Results on different subjects in the theme of Fig. 6.

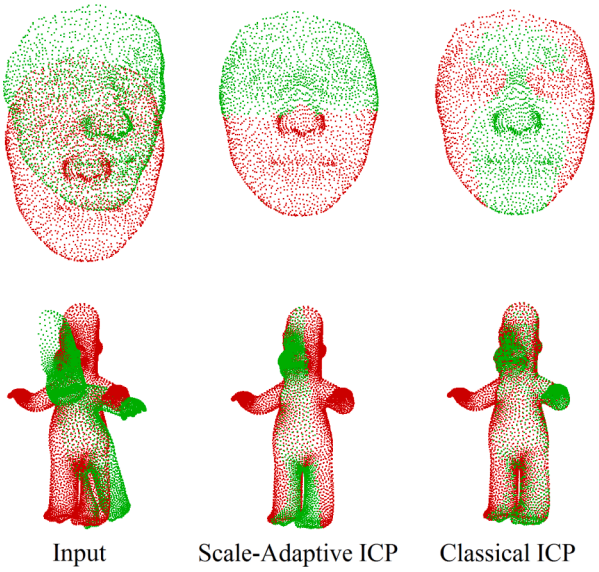

Fig. 8. Alignments of pairs with compatible initial scaling.

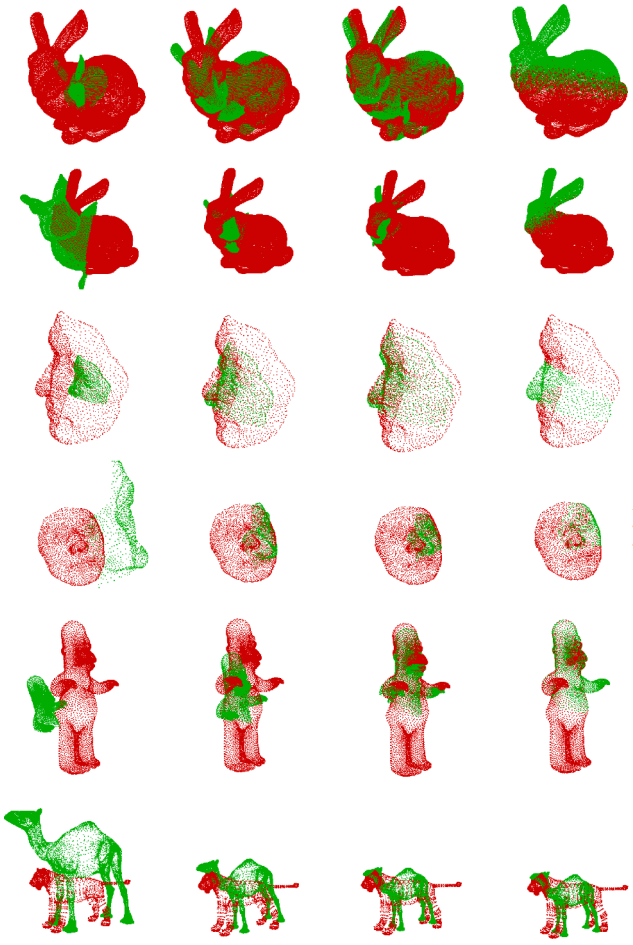

Fig. 9. Progress of our scale-adaptive ICP algorithm. All intermediate steps for these pairs and many others are available in the supplementary video.

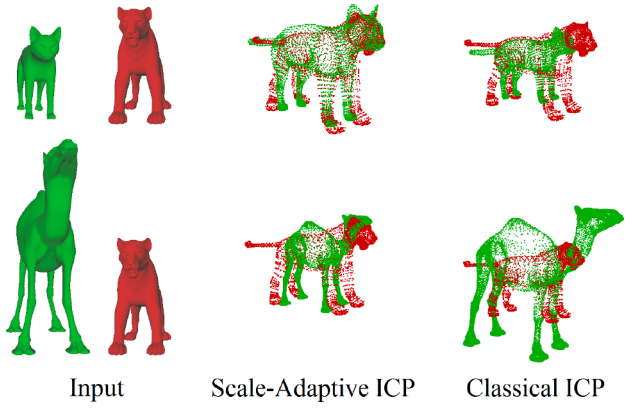

Fig. 10. Our alignment of non-rigid shape pairs cat-lion and camel-lion provides a better initialization for an upcoming non-rigid registration operation.

As another quantitative assessment, we provide timing measured on an 8GB 3.4GHz 64-bit PC (Table 3). Full means all points are aligned, e.g., Fig. 7-first row, whereas partial means a cropped version is aligned, e.g., Fig. 7-second row. Note that Face, Bunny, Homer, and Quadrupeds have 2639, 34835, 7506, and 11,062 points, respectively. When aligning n points towards a fixed set of m points, the time complexity of each scale-adaptive ICP iteration is $O(n \log m)$ with a k-d tree being used for the closest point computations. Timing of TEASER [45], on the other hand, is obtained on a different machine, namely a MacBook Pro-with

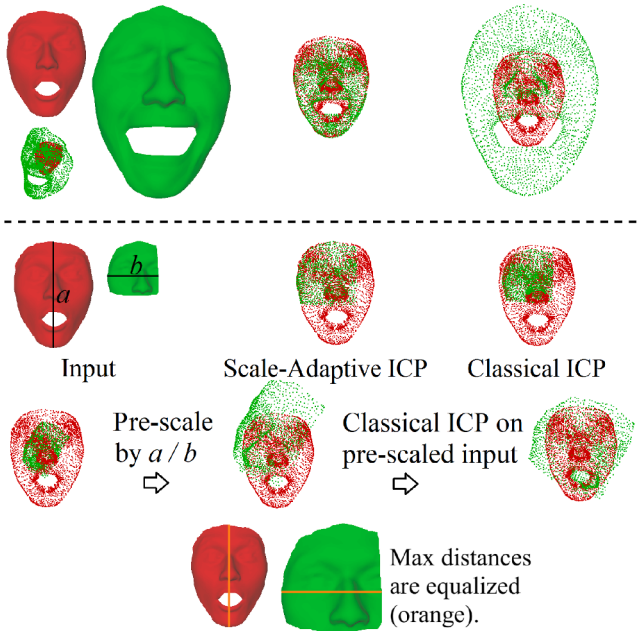

Fig. 11. (Above the dashed line) A non-rigid shape pair is aligned with our scale-adaptive ICP (middle) and classical ICP (right). Initial configuration is given in the bottom of the shaded red shape. (Below the dashed line) Another non-rigid pair is aligned. For this pair, we also show the shortcoming of the naïve distance-based pre-scaling (described in Fig. 1) at the rows below. The shaded versions of the pre-scaled shapes are also given for visual convenience. Note that the maximum distances in orange become equal after scale normalization, which, however, does not yield a proper global scaling since the most widely separated point pairs that define the maximum distances do not correspond semantically. (For interpretation of the references to colour in this figure legend, the reader is referred to the web version of this article.)

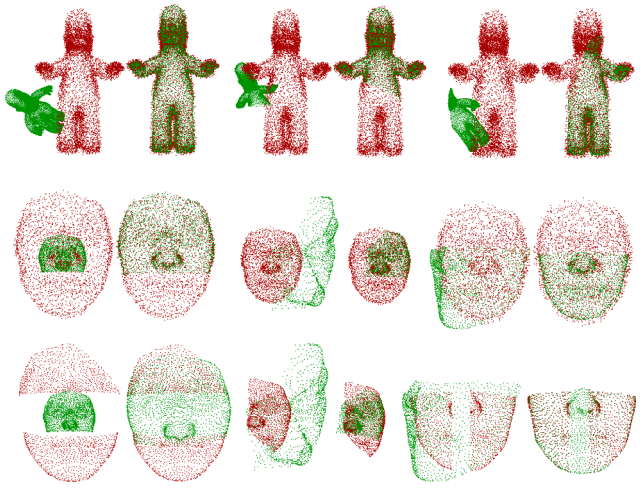

Fig. 12. Our results under geometric noise (rows 1–2) and extended partiality where the red target also cropped (row 3). (For interpretation of the references to colour in this figure legend, the reader is referred to the web version of this article.)

Table 2
Eq. 1 error of our results under noise and extreme partiality.

	Face	Bunny	Homer	Quadrupeds
Noise	0.00025	0.00021	0.00017	0.00338
E-Partiality	0.11051	0.16526	0.13789	0.19973

Table 3
Execution time of our method (seconds:#iterations). Note that timing of the classical ICP [4] is exactly the same since the additional linear system we solve has a constant size (Eq. 6).

	Face	Bunny	Homer	Quadrupeds
Full	1.55:33	14.18:35	3.51:26	3.65:31
Partial	1.91:57	8.29:24	2.42:20	2.64:19

2.9 GHz 6-Core Intel Core i9, using 12 threads. In this configuration, TEASER requires 400 matches for partial Bunny and 300 for partial Homer and Face cases. This matching operation takes under a second and then followed by 1 second of scale, rotation, translation computation for the partial Bunny, and 0.5 seconds for the partial Homer and Face. Note that, TEASER can work with any robust matching algorithm. Currently, authors have used a parallel implementation of FPFH which is 16x faster than a sequential implementation [16,18].

5. Limitations

Out of 20 test pairs per category, failure cases occasionally arose. Although our algorithm completes with almost zero alignment error (Eq. 1) in these cases, the result might be semantically incorrect, e.g., shifted towards a place that is good for alignment error but bad for semantic meaning (Fig. 13). This shifting problem depends on not only the initial scale difference but also the initial positioning of the two point sets. We are thus unable to provide a proper quantitative analysis that reveals the relationship between the relative scale and convergence behavior. We observed the problematic cases 4, 2, 1, and 6 times for the Face, Bunny, Homer, and Quadruped categories, respectively. While providing merely 3 ground-truth correspondences resolves all the issues, it would still be a strong assumption to have this information. Design of a scale-invariant point descriptor can lead to an automatic solution to this issue, an interesting future research direction to follow.

6. Conclusion and future work

We presented scale-adaptive iterative closest point algorithm for robust pairwise alignment under arbitrary scaling. To this effect, we jointly optimize for translation and scaling after the application of the optimal rotation. The proposed joint optimization boils down to a small linear system that is solved instantly. We demonstrated clear advantages of our algorithm through comparisons involving the correspondence-free pre-scaling methods that precede the classical ICP, the current state-of-the-art method that decouples scale estimation via correspondences, and a baseline method that adds the scaling factor into the optimization.

It can be interesting to support non-uniform scaling, which requires optimization of three scaling factors instead of just one. Sparse modeling techniques [5,26] may help dealing with significant amounts of noise and outliers. We also consider incorporation of a novel scale-invariant point descriptor to our framework (Section 5) as another future research direction.

Funding

Funding was received for this work.

All of the sources of funding for the work described in this publication are acknowledged below:

[List funding sources and their role in study design, data analysis, and result interpretation]

TUBITAK project EEEAG-115E471

NSF projects IIS-1617172, IIS-1622360, and IIS-1764071.

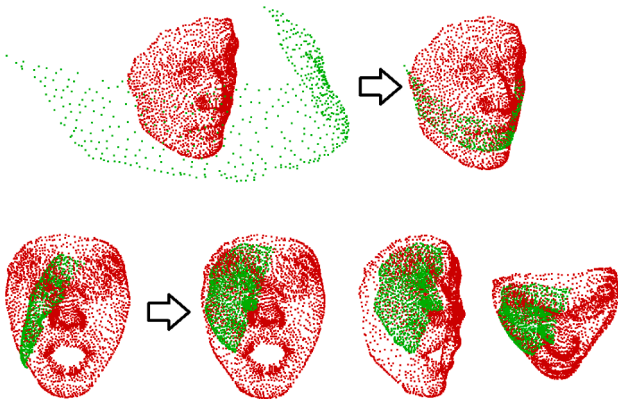

Fig. 13. Two failure cases of the face category. Multiple views are provided for the second one for visual convenience.

Intellectual Property

We confirm that we have given due consideration to the protection of intellectual property associated with this work and that there are no impediments to publication, including the timing of publication, with respect to intellectual property. In so doing we confirm that we have followed the regulations of our institutions concerning intellectual property.

Research Ethics

We further confirm that any aspect of the work covered in this manuscript that has involved human patients has been conducted with the ethical approval of all relevant bodies and that such approvals are acknowledged within the manuscript.

Authorship

All listed authors meet the ICMJE criteria. We attest that all authors contributed significantly to the creation of this manuscript, each having fulfilled criteria as established by the ICMJE.

We confirm that the manuscript has been read and approved by all named authors.

We confirm that the order of authors listed in the manuscript has been approved by all named authors.

Contact with the Editorial Office

This author submitted this manuscript using his/her account in editorial submission system.

We understand that this Corresponding Author is the sole contact for the Editorial process (including the editorial submission system and direct communications with the office). He/she is responsible for communicating with the other authors about progress, submissions of revisions and final approval of proofs.

We confirm that the email address shown below is accessible by the Corresponding Author, is the address to which Corresponding Author editorial submission system account is linked, and has been configured to accept email from the editorial office of International Journal of Women Dermatology: [Insert email address you wish to use for communication with the journal here] ysahillioglu@gmail.com

Declaration of Competing Interest

The authors declare that they have no known competing financial interests or personal relationships that could have appeared to influence the work reported in this paper.

Acknowlgedgments

We thank the anonymous reviewers for their comments and Heng Yang for the help with his paper's experiments.

Supplementary material

Supplementary material associated with this article can be found, in the online version, at 10.1016/j.gmod.2021.101113

References

[1] D. Aiger, N.J. Mitra, D. Cohen-Or, 4-points congruent sets for robust pairwise surface registration. ACM transactions on graphics (TOG) 27, Acm, 2008, p. 85.
[2] C. Basdogan, A.C. Oztireli, A new feature-based method for robust and efficient rigid-body registration of overlapping point clouds, Vis Comput 24 (7–9) (2008) 679–688.
[3] H. Bay, A. Ess, T. Tuytelaars, L. Van Gool, Speeded-up robust features (surf), Comput. Vision Image Understanding 110 (3) (2008) 346–359.
[4] P.J. Besl, N.D. McKay, Method for registration of 3-d shapes. Sensor fusion IV: control paradigms and data structures 1611, International Society for Optics and Photonics, 1992, pp. 586–606.
[5] S. Bouaziz, A. Tagliasacchi, M. Pauly, Sparse iterative closest point. Proceedings of the Eleventh Eurographics/ACMSIGGRAPH Symposium on Geometry Processing, Eurographics Association, 2013, pp. 113–123.
[6] D. Ceylan, N.J. Mitra, Y. Zheng, M. Pauly, Coupled structure-from-motion and 3d symmetry detection for urban facades, ACM Transactions on Graphics (TOG) 33 (1) (2014) 2.
[7] W. Chang, M. Zwicker, Range scan registration using reduced deformable models, Comput. Graphics Forum 28 (2) (2009) 447–456.
[8] Y. Chen, G. Medioni, Object modelling by registration of multiple range images, Image Vis Comput 10 (3) (1992) 145–155.
[9] C. Choy, J. Park, V. Koltun, Fully convolutional geometric features. Proceedings of the IEEE International Conference on Computer Vision, 2019, pp. 8958–8966.
[10] Y. Diez, F. Roure, X. Lladó, J. Salvi, A qualitative review on 3d coarse registration methods, ACM Comput Surv 47 (3) (2015) 45.
[11] S. Du, J. Liu, B. Bi, J. Zhu, J. Xue, New iterative closest point algorithm for isotropic scaling registration of point sets with noise, Journal of Visual Comm. and Image Rep. 38 (2016) 207–216.
[12] S. Du, N. Zheng, L. Xiong, S. Ying, J. Xue, Scaling iterative closest point algorithm for registration of m–d point sets, J Vis Commun Image Represent 21 (5–6) (2010) 442–452.
[13] S. Du, N. Zheng, S. Ying, Q. You, Y. Wu, An extension of the icp algorithm considering scale factor. 2007 IEEE International Conference on Image Processing 5, IEEE, 2007, pp. V–193.
[14] J. Ekekrantz, A. Pronobis, J. Folkesson, P. Jensfelt, Adaptive iterative closest keypoint. 2013 European conference on mobile robots, IEEE, 2013, pp. 80–87.
[15] G. Elbaz, T. Avraham, A. Fischer, 3d point cloud registration for localization using a deep neural network auto-encoder. Proceedings of the IEEE Conference on Computer Vision and Pattern Recognition, 2017, pp. 4631–4640.
[16] T. Garrett, R. Radkowski, J. Sheaffer, Gpu-accelerated descriptor extraction process for 3d registration in augmented reality. International Conference on Pattern Recognition, 2016, pp. 3085–3090.
[17] Z. Gojcic, C. Zhou, J.D. Wegner, A. Wieser, The perfect match: 3d point cloud matching with smoothed densities. Proceedings of the IEEE Conference on Computer Vision and Pattern Recognition, 2019, pp. 5545–5554.
[18] Z. Gojcic, C. Zhou, J.D. Wegner, A. Wieser, The perfect match: 3d point cloud matching with smoothed densities. Proceedings of the IEEE/CVF Conference on Computer Vision and Pattern Recognition, 2019, pp. 5545–5554.
[19] B. Horn, Closed-form solution of absolute orientation using unit quaternions, JOSA A 4 (4) (1987) 629–642.
[20] T. Jost, H. Hugli, A multi-resolution icp with heuristic closest point search for fast and robust 3d registration of range images. Fourth International Conference on 3-D Digital Imaging and Modeling, 2003. 3DIM 2003. Proceedings., IEEE, 2003, pp. 427–433.
[21] M. Khoury, Q.-Y. Zhou, V. Koltun, Learning compact geometric features. Proceedings of the IEEE International Conference on Computer Vision, 2017, pp. 153–161.
[22] C. Li, J. Xue, N. Zheng, S. Du, J. Zhu, Z. Tian, Fast and robust isotropic scaling iterative closest point algorithm. 2011 18th IEEE International Conference on Image Processing, 2011, pp. 1485–1488.
[23] H. Li, E. Vouga, A. Gudym, L. Luo, J.T. Barron, G. Gusev, 3D self-portraits, ACM Transactions on Graphics (TOG) 32 (6) (2013) 187.
[24] B. Lin, T. Tamaki, B. Raytchev, K. Kaneda, K. Ichii, Scale ratio icp for 3d point clouds with different scales. 2013 IEEE International Conference on Image Processing, IEEE, 2013, pp. 2217–2221.
[25] B. Lin, T. Tamaki, F. Zhao, B. Raytchev, K. Kaneda, K. Ichii, Scale alignment of 3d point clouds with different scales, Mach Vis Appl 25 (8) (2014) 1989–2002.
[26] P. Mavridis, A. Andreadis, G. Papaioannou, Efficient sparse icp, Comput Aided Geom Des 35 (2015) 16–26.
[27] N. Mellado, D. Aiger, N.J. Mitra, Super 4pcs fast global pointcloud registration via smart indexing. Computer Graphics Forum 33, Wiley Online Library, 2014, pp. 205–215.
[28] N. Mellado, M. Dellepiane, R. Scopigno, Relative scale estimation and 3d registration of multi-modal geometry using growing least squares, Trans. on Visual. and Comp. Graph. 22 (9) (2015) 2160–2173.
[29] C. Miller, O. Arikan, D.S. Fussell, Frankenrigs: building character rigs from multiple sources, IEEE Trans Vis Comput Graph 17 (8) (2011) 1060–1070.
[30] M. Mohamad, M.T. Ahmed, D. Rappaport, M. Greenspan, Super generalized 4pcs for 3d registration. 2015 International Conference on 3D Vision, IEEE, 2015, pp. 598–606.
[31] C. Olsson, F. Kahl, M. Oskarsson, Branch-and-bound methods for euclidean registration problems, IEEE Trans Pattern Anal Mach Intell 31 (5) (2008) 783–794.
[32] H. Pottmann, J. Wallner, Q.-X. Huang, Y.-L. Yang, Integral invariants for robust geometry processing, Comput Aided Geom Des 26 (1) (2009) 37–60.
[33] E. Rublee, V. Rabaud, K. Konolige, G. Bradski, Orb: An efficient alternative to sift or surf. 2011 International conference on computer vision, Ieee, 2011, pp. 2564–2571.
[34] S. Rusinkiewicz, A symmetric objective function for ICP, ACM Transactions on Graphics (Proc. SIGGRAPH) 38 (4) (2019).
[35] S. Rusinkiewicz, M. Levoy, Efficient variants of the icp algorithm.. 3dim 1, 2001, pp. 145–152.
[36] R.B. Rusu, N. Blodow, M. Beetz, Fast point feature histograms (fpfh) for 3d registration. 2009 IEEE international conference on robotics and automation, IEEE, 2009, pp. 3212–3217.
[37] Y. Sahillioğlu, Y. Yemez, Scale normalization for isometric shape matching. Computer Graphics Forum 31, Wiley Online Library, 2012, pp. 2233–2240.
[38] Y. Sahillioğlu, L. Kavan, Skuller: a volumetric shape registration algorithm for modeling skull deformities, Med Image Anal 23 (1) (2015) 15–27.
[39] L. Silva, O.R.P. Bellon, K.L. Boyer, Precision range image registration using a robust surface interpenetration measure and enhanced genetic algorithms, IEEE Trans Pattern Anal Mach Intell 27 (5) (2005) 762–776.
[40] R.W. Sumner, J. Popović, Deformation transfer for triangle meshes, ACM Transactions on graphics (TOG) 23 (3) (2004) 399–405.
[41] G.K. Tam, Z.-Q. Cheng, Y.-K. Lai, F.C. Langbein, Y. Liu, D. Marshall, R.R. Martin, X.-F. Sun, P.L. Rosin, Registration of 3d point clouds and meshes: a survey from rigid to nonrigid, IEEE Trans Vis Comput Graph 19 (7) (2012) 1199–1217.
[42] T. Tamaki, S. Tanigawa, Y. Ueno, B. Raytchev, K. Kaneda, Scale matching of 3d point clouds by finding keyscales with spin images. 2010 20th International Conference on Pattern Recognition, IEEE, 2010, pp. 3480–3483.
[43] Z. Wu, H. Chen, S. Du, M. Fu, N. Zhou, N. Zheng, Correntropy based scale icp algorithm for robust point set registration, Pattern Recognit 93 (2019) 14–24.
[44] H. Yang, L. Carlone, A polynomial-time solution for robust registration with extreme outlier rates. In Robotics: Science and Systems (RSS), 2019.
[45] H. Yang, J. Shi, L. Carlone, TEASER: Fast and certifiable point cloud registration, IEEE Trans. Robotics (2020).
[46] J. Yang, H. Li, D. Campbell, Y. Jia, Go-icp: a globally optimal solution to 3d icp point-set registration, IEEE Trans Pattern Anal Mach Intell 38 (11) (2015) 2241–2254.
[47] Z.J. Yew, G.H. Lee, 3dfeat-net: Weakly supervised local 3d features for point cloud registration. European Conference on Computer Vision, Springer, 2018, pp. 630–646.
[48] S. Ying, J. Peng, S. Du, H. Qiao, A scale stretch method based on icp for 3d data registration, IEEE Trans. Autom. Sci. Eng. 6 (3) (2009) 559–565.
[49] A. Zeng, S. Song, M. Nießner, M. Fisher, J. Xiao, T. Funkhouser, 3dmatch: Learning local geometric descriptors from rgb-d reconstructions. CVPR, 2017.
[50] Q.-Y. Zhou, J. Park, V. Koltun, Fast global registration. European Conference on Computer Vision, Springer, 2016, pp. 766–782.
[51] A. Zia, J. Liang, J. Zhou, Y. Gao, 3d reconstruction from hyperspectral images. 2015 IEEE Winter Conference on Applications of Computer Vision, IEEE, 2015, pp. 318–325.
[52] T. Zinßer, J. Schmidt, H. Niemann, Point set registration with integrated scale estimation. International conference on pattern recognition and image processing, 2005, pp. 116–119.

Yusuf Sahillioğlu is an associate professor in the Department of Computer Engineering at Middle East Technical University. He is also an associate editor of The Visual Computer journal. His research interests include digital geometry processing and computer graphics. He has a PhD in computer science from Koç University, Turkey. Contact him at ys@ceng.metu.edu.tr or visit http://www.ceng.metu.edu.tr/~ys.